JOINT EUROPEAN TORUS

JET–P(91)41

V.P. Bhatnagar, J. Jacquinot, D.F.H Start
and JET Team

Fast-Wave Current-Drive Efficiency Calculations for JET A2-Antennas

Fast-Wave Current-Drive Efficiency Calculations for JET A2-Antennas

V.P. Bhatnagar, J. Jacquinot, D.F.H Start
and JET Team*

JET-Joint Undertaking, Culham Science Centre, OX14 3DB, Abingdon, UK

** See Appendix 1*

Paper presented at the IAEA Technical Committee Meeting on
FWCD in Reactor Scale Tokamaks, Aries, France, September 23-25, 1991

FAST-WAVE CURRENT-DRIVE EFFICIENCY CALCULATIONS FOR JET A2-ANTENNAS

V.P. Bhatnagar, J. Jacquinot, D.F.H. Start

JET Joint Undertaking, Abingdon, Oxfordshire, England OX14 3EA

ABSTRACT

Fast-wave transit-time magnetic-pumping (TTMP) current drive efficiency calculations using ray tracing techniques are presented using A2-antennas for the experiments to be carried out in the divertor phase of the extended JET programme. The antenna plasma coupling problem is properly solved using a full wave solution which allows to incorporate the antenna array directivity and full asymmetric spectrum in the calculations. Current drive calculation at each step of the ray allows to take into account the power deposition profile and the electron trapping effects correctly. The poloidal field effects which change $k_{//}$ and therefore have important consequences on the current drive efficiencies are also taken into account. It is shown that current drive efficiency factor $\gamma \cong 0.11$ in units of $10^{20} W/A/m^2$ is obtained for an electron temperature of 10 keV. Synergistic effects between the ICRH and the lower hybrid current drive system in which a population of fast electrons ($\cong 100 - 200 keV$) is produced is also evaluated. It is found that a 0.5% concentration of 200 keV fast electrons would increase the current drive efficiency by 35% at a toroidal mode number n = 11 and this increase could be as large as a factor of 2 at lower n = 2-4.

1. INTRODUCTION.

Designers of next-step tokamak devices appear to embrace preferentially only those additional heating schemes that have demonstrated or have a good potential for non inductive current drive. This is because the latter appears to be essential for continous operation of a tokamak reactor, though an alternative scheme, using alternating current (AC) operation has recently been experimentally demonstrated in the JET toakamak [1]. Fast magnetosonic waves in the ion cyclotron range of frequencies are now being increasingly acclaimed as a leading candidate for non inductive current drive in reactor-grade plasmas. This is due to the fact that potentially the fast waves can be used with parallel phase velocities up to the speed of light enjoying higher efficiencies (current drive efficiency $\propto v^2_{//}$), and can drive current in the centre as they have no limitation of penetrating to the centre of a high density, high temperature reactor plasma and are not subject to any density limit. Current drive schemes using fast waves to accelerate electrons can be classified according to whether the absorption is dominated by electron Landau damping (ELD) or if the transit time magnetic pumping (TTMP) plays a major role. Using fast waves at lower frequencies ($\omega \leq \omega_{ci}$) in plasmas of high electron β (ratio of kinetic

to magnetic pressure) such that the Moreau [2] parameter $\alpha \equiv T_e(\omega_{pi}/\omega)^2 = 10 - 50$, the TTMP is the dominant component in the damping process.

Though TTMP current drive experiments have not yet been carried out, but a clear observation of the fast wave electron damping has been made [3,4]. The disadvantage of the TTMP scheme for present size experiments, and the reason for its slow experimental evaluation, is the weak damping relative to other absorption mechanisms, such as the ion cyclotron damping. However, significant TTMP current drive experiments are now underway [5,6] or are planned at JET [7] to be carried out in the divertor phase of the JET extended programme. For the pumped-divertor phase of JET, a new set of four ICRH antennas (A2) are being constructed with four current straps in each antenna to increase the directivity of the phased array. These antennas will be used both for heating and current drive experiments in JET with appropriate phasing between the straps. A significant effort is being devoted to arbitrarily phase and match the antenna array [7,8,9] keeping the current in different straps constant and to deal successfully with the circulating power which is injurious to the generator tube system. The automatic VSWR control system [10] of JET has permitted the matching of a coupled pair of straps in an antenna with arbitrary phasing [7] when the current $|I|$ in both straps is maintained equal. In this operation $\cong 5MW$ of ICRH power has been coupled to JET plasmas using four A1-antennas (2-straps each) in a minority ion current drive scenario [11].

In this paper, we use the ray tracing technique to calculate the current drive effciency of JET A2-antennas. First, we analyse the excitation of the fast wave by an ICRH antenna array in a semi-infinite planar model to calculate the loading resistance of the array, the directivity of the excited spectrum and initial conditions for ray tracing calculations. The ray tracing equations are then solved in 3-dimensions in a JET D-shaped plasma. The poloidal field effects (which change $k_{//}$), and therefore have important consequences on the current drive efficiencies, are taken into account. At each step of the ray, the normalized current drive efficiency $\eta = j_n/p_n$ is calculated by a bounce averaged Fokker-Planck theory. Here, j_n and p_n are respectively the normalized current density and absorbed power density. The elemental current driven is then obtained knowing the absorbed power at each step. This procedure thus allows to take the effect of particle trapping correctly into account. These calculations for JET predict a current drive efficiency factor γ ($= <n_e> I\ R_0/P$) of about 0.11 (in units of 10^{20}A/W/m^2). In the above, $<n_e>$ is the volume average density, I is the driven current, R_0 is the major radius and P is the power absorbed by electrons.

Recent lower hybrid experiments ($n_{//} \cong 2$) combined with ICRH in JET have indicated a synergistic effect in which the fast electrons [12,13] ($\cong 100 - 200keV$) produced by the lower hybrid current drive (LHCD) sytem are further accelerated by the ICRH power spectrum excited by a monopole antenna which overlaps the lower hybrid spectrum. In view of this result, we have made further calculations of current drive efficiencies for A2-antennas in which fast electrons (200 keV) with a concentration of about 0.5% are assumed to be present in the plasma. Results show that there is an increased power absorption by TTMP by this fast electron population and the current drive efficiency increases by about 35% when the preferentially excited toroidal mode number (n) is 11 (or $k_{//} \cong 2.5m^{-1}$). This increase can be even higher (a factor of $\cong 2$) at lower n = 2-3 where the dominant excited spectrum is more close to that resonating with the fast electron population present.

2. RAY TRACING CALCULATION OF CURRENT DRIVE.

2.1 General Remarks: The theory of non inductive current drive in a tokamak, generally, requires the solution of a bounce-averaged Fokker-Planck equation. Quasilinear theory can deal with the collisionless interaction of RF waves with a plasma and RF effects can be included by a quasilinear ICRF diffusion operator. This provides appropriate distribution functions from which averages of macroscopic variables can be deduced by integration and the efficiency of RF current current drive can be calculated. However, to be consistent in solving the Fokker-Planck equation, one must solve for the linear wave field by a full-wave solution in toroidal geometry for a given antenna array that is phased to provide an asymmetric $k_{//}$-spectrum. Such a spectrum is necessary for providing the asymmetry in velocity space of the RF operator responsible for current drive. The calculated directivity can then also be included in the results of current drive efficiencies.

The full-wave solution of ICRF wave fields in a hot toroidal plasma has been attempted by several numerical codes LION [14], ALCYON [15], SPRUCE [16] etc. either using finite-difference or finite element techniques. However, these codes do not include the effect of poloidal field and often run into difficulties with the grid size and also the memory required (1) for large plasmas (reactor-size machines) and (2) to resolve certain phenonemon, for example, mode conversion. In the following we use the ray tracing technique, although it does not treat the problem of eigen modes that may be present in the weak absorption limit, it can provide rapid answers, as a first approximation, with the essential physics included such as the important effect of poloidal field and change of $k_{//}$. We solve the antenna-plasma coupling problem by a full-wave solution in the edge plasma region, and by appropriately matching it to the geometric optics solution, we carry out the ray tracing in the central hot plasma region where the absorption takes place and calculate the current drive efficiencies at each step of ray tracing by analytic fits to more complete Fokker-Planck numerical codes. Power absorption and current drive profiles in a non circular tokamak plasma are also generated.

2.2 A2-Antenna and its Layout: A perspective view of four straps of A2-antenna [20] and its associated components are shown in Fig. 1. A single tier of beryllium rods inclined at varying angles ($\cong 15°$) along its length from the toroidal direction are used as an electrostatic screen to filter out the slow wave. A relatively open screen gives low RF losses and enables cooling by radiation alone. The increased projection of the antenna into the torus, due to reduced plasma size to accomodate the divertor coils, has severely increased the predicted plasma disruption forces on the antenna structure. Therefore, the main antenna housing is of of an uncoventional design using thin corrugated sheet metal construction with multiple fixation to the torus. The central conductor is made from a thick rigid tubular frame onto which a thin sheet is welded. Each screen element carries a specially designed resistor in series to reduce the DC current in the screen rods without increasing the RF losses. A septum slotted to a depth of about 1/3 separates adjacent current straps. The toroidal location of antennas is shown in Fig. 2. The antennas are arranged in pairs (such that they are clear from the NBI beam paths) with each antenna structure having equi-pitched four straps as shown.

2.3 Antenna-Plasma Coupling: We analyse the excitation of fast wave by an ICRH antenna array in a semi-infinite (strong damping and no reflected wave), planar (antenna length smaller than the plasma height), cold (edge) plasma model

with finite width and length of an antenna element. The detail of this model has been given elsewhere [17,18] but, here we point out that analysis of this model gives (1) the radiation resistance of the antenna array, (2) the directivity, (3) asymmetric $k_{//}$-spectrum and (4) the initial conditions for starting ray tracing from a plasma region where WKB-assumptions are satisfied. These initial conditions are obtained from a partial-wave [19] analysis for an array of antennas.

2.3.1 Directivity: Now we present the results of directivity of the JET A2-antenna array to be used for the current drive experiments. The directivity is defined as

$$D = \sum_{n=1}^{n} \frac{P(n) - P(-n)}{P_{tot}}$$

where n is the toroidal mode number and P represents the power in that particular mode number. The parallel propagation constant is $k_{//} = n/R_a$ where R_a is the major radius of the antenna array location in the tokamak. Using the antenna plasma coupling code mentioned above, the calculated directivity of A2-antenna array is shown in Fig. 3 as a function of n (or $k_{//}$) when the antennas are phased progressively to produce a travelling wave. The antenna and the plasma parameters used are given in Table 1. Plasma parameters used are typical of JET discharges. The phase difference between two successive straps is given by $\Delta\phi(rad) = (n/R_a)L_z$. The maximum directivity of 0.88 is obtained for n = 11 and is related to the phasing of four successive straps in the array. The middle to middle distance between adjacent straps toroidally is $L_z = 0.4$ m. Note that this array of four straps is not uniformly placed around the torus but is grouped into two which leads to a small dip in the directivity at n = 3-5. In Fig. 3 we also plot the parallel energy of electrons that will be resonant with a given mode number n (or $k_{//}$) when f = 35 MHz and $v_e = \sqrt{2E_{//}/m}$. Here, $k_0 \equiv \omega/c = 0.73$ and $n_{//} = c/v_e = k_{//}/k_0$ where c is the speed of light.

2.3.2 Power Spectrum: We illustrate the excited spectrum of the above antenna array in Fig. 4 in which phasing was done to excite n = 11 predominantly. Compared to the spectrum of a single antenna (which is a convolution of the plasma response and the Fourier current spectrum of the antenna) a narrowing and quantization of the spectrum occurs as the number of antennas is increased. For symmetrically placed antennas around the torus the spectrum and the directivity can be obtained analytically based on the antenna array factor as discussed in Ref. 21. In the spectrum shown, there is a significant amount of power in mode numbers other than n = 11. The higher $k_{//}$ part of the spectrum would also be useful for heating whereas the lower $k_{//}$ part can resonate with the fast electron population produced by LHCD system. However, to resonate more strongly with fast electrons, lower n = 3 to 5 should be excited.

2.4 Ray Tracing and Fokker-Planck Treatment: Away from the fast-wave evanescent region of the plasma, where the geometric optics approximation is valid, ray tracing equations [22] are solved in 3-dimensions for multispecies plasma with arbitrary density and temperature profiles. Both toroidal and poloidal components of the magnetic field and their profiles are taken into account including the variation of $k_{//}$ due to the poloidal field which is of considerable importance in damping and current drive efficiency calculations. Power absorbed by different species along the ray path is computed using a hot plasma description which contains ELD, e-TTMP

and, fundamental and second harmonic dampings. The non circular (D-shape) tokamak geometry is described analytically in terms of elongation, triangularity and Shafranov shift of the magnetic axis. In order to generate absorption and current-drive profiles, we subdivide the plasma into a certain number of annular regions similar to magnetic surfaces. Starting at a flux surface, typically 50 rays are launched from several poloidal locations that encompasses the excited $k_{//}$-power spectrum weighted by the square of the antenna current variation in the poloidal direction. Ray tracing is continued for multiple passes until the power left in a ray is below a desired value. As a ray advances, power deposited in each layer is accumulated. At each step of the ray, the normalized current drive efficiency $\eta = j_n/p_n$ is calculated by the bounce averaged Fokker-Planck theory [23]. Here, j_n and p_n are respectively the normalized (see, for example, Ref. [24]) current density and absorbed power density. However, note that v_{th} is defined as $\sqrt{T_e/m}$. In practical units, we find that [24]

$$\frac{I(amps)}{P(watt)} = 3.05.10^{18}.\frac{T_e(keV)}{R(m)n_e(m^{-3})\ln\Lambda}.\eta$$

where R is the major radius and ln Λ is the Coulomb logrithm. The elemental driven current is obtained by the product of the quantity on the right hand side and the power absorbed in a ray tracing step. The elemental current in each layer is also accumulated. Calculation at each step allows to take into account the power absorption profile and the trapping effects correctly. Finally, the power depostion profile and the current drive profiles are generated by a flux surface averaging of the two quantities.

The details of the calculation of η and the model used are given in Ref. 23. However, in order to reduce the computation time, we have found the use of an analytic fit due to Ehst [25] much more convenient. The analytic fit has been checked against the numerical results of Ref. 26 within an accuracy of $\pm$ 12% and succesfully reproduces the effects such as : (1) the current drive efficiency decreases with ξ ($= v_{ph}/v_{th}$) for low ξ reaches a minimum at about $\xi = 1$ and then increases with ξ, (2) the effect of trapping reduces with decreasing inverse aspect ratio, (3) Effect of trapping is small for large values of ξ, but increases dramatically for $\xi < 1$ for particles on the low-field side and (4) current drive efficiency reduces with increasing Z_{eff} etc.

2.4.1 CD efficiency without Fast Electron Population: Based on the above model, we present the results of current drive efficiency factor γ as a function of the toroidal mode number n for the JET A2-antenna array in Fig. 5 where we assume that $T_{e0} = 10$ keV and $Z_{eff} = 1$. The other parameters are as given in Table 1. We find that maximum value of $\gamma \equiv < n_e > IR_0/P$ is about $0.11 \cdot 10^{20} A/W/m^2$ at n = 11. These results shown by the line drawn through the circles in the figure reflect approximately the directivity of the antenna except that the current drive efficiency is slightly superior at lower n = 3-5. The other results are computed with a fast electron population and are dicussed in the next section.

2.4.2 CD Efficiency in the Presence of a Fast Electron Population: As mentioned in the Introduction, the LHCD system produces a fast electron population which can be acclerated synergistically by the low $k_{//}$ spectrum excited by the ICRH monopole antenna. However, here we will not deal with the self consistent production of the fast electron population by the LHCD system but will introduce into our computations another electron species having a Maxwellian temperature of 200 keV in the centre. The concentration of this species is not exactly known experimentally but can be estimated by consistency arguments of the current driven by the fast

electron species or by matching the measured electron distribution function with a calculated two temperature two species distribution function. For about 2 MW of LHCD power in low density JET plasmas, these estimates give a concentration of about 0.25 to 0.5% of the bulk electron population. However, in our theoretical results we shall vary this parameter from 0 to 5%. In Fig. 6, we present the relative power absorbed by the bulk electrons ($T_{e0} = 10keV$) and that by isotropic fast electrons ($T_{fe0} = 200keV$) as a function of the concentration of these fast electrons. The antenna array was phased to excite n = 10. In these calculations, the background ion resonances have been placed in the cold region near the edge of the plasma. The ray tracing is continued for 3 to 5 passes and the unabsorbed power is assumed to be absorbed in the same proportion as in first 3-5 passes. It is seen that the power absorbed by fast electrons increases as their concentration is increased and equal amount of power is absorbed when $n_e(200keV)/n_e = 0.013$. In such a condition, single pass absorption by electrons including that by fast electrons is about 15%. The current drive efficiency factor γ plotted as a function of the concentration of fast electron population for n = 10 is shown in Fig. 7. It is found that the major increase in the value of γ occurs already at low concentration (≤ 0.01) and then it increases slowly. The increase in γ in the presence of fast electrons is related to the increased power absorption and the increased efficiency in current drive of the lower part of the $k_{//}$ spectrum resonant with fast electrons. However, for n = 10, the power in the lower spectrum is only about 15-20% and no large increase in efficiencies can be expected.

Now, we fix the concentration of fast electrons to 0.5% and calculate γ as a function of n and the results are shown in Fig. 5 where they are compared to the case without fast electrons as discussed in the last section. The values of γ shown in Fig. 5 at lower n numbers ($n \leq 3$) are overestimated as no relativistic corrections were applied. The efficiencies would level off when the phase velocity approaches the speed of light. We find that γ increases by about 35% for n = 11 but it increases by a larger factor (≤ 2 when estimates of relativistic corrections are duly taken into account) for n = 2-3 as a larger fraction of the spectrum is resonant with fast electrons.

In Fig. 8, we show the electron power deposition profile as absorbed by bulk electrons and the 200 keV fast electrons where their concentration was 0.5%. Due to weak single pass damping ($\cong 7\%$), the power deposition profile is somewhat broad. The noninductive current drive profile is shown in Fig. 9 where with an input power of 2.55 MW absorbed in the electrons, the total current driven is 0.57 MA at a central density of $5 \cdot 10^{19} m^{-3}$ in the presence of 0.5% of fast electrons (200 keV) in the central region of the plasma.

3. DISCUSSION AND CONCLUSION.

In this paper we have presented ray tracing calculations of current drive by ICRF waves due to e-TTMP and ELD damping for the experiments to be carried out in the divertor phase of the JET tokamak with 4x4 straps of the A2-antenna array. Ray tracing does not take into account the eigen modes that may be present in the plasma due to weak damping of the wave. In the present version of the code, damping at the Alfven resonance is also not included, although some estimates could be obtained based on the Budden formulation. Full-wave codes also seem to run into problems to resolve such localised absorptions due to the very fine grid required. In ray tracing, the effect of poloidal field on the current drive efficiency has been properly taken into account [27]. Also, the antenna array and its excited $k_{//}$-spectrum and directivity has been appropriately calculated. Note that in these calculations, tokamak equilibrium has not been self-consistently determined where the effect of

RF driven current and the bootstrap current has to be taken into account in addition to the ohmic current drive. Also, we have not considered the effect of radial transport of electrons which is likely to reduce the current drive efficiency [28]. Finally, we have not dealt with the problem of LHCD produced fast electron tail self-consistently. The evaluation of synergistic effects, therefore, must take into account the power required to sustain such a tail.

In **conclusion,** we have shown that with JET A2-antennas, TTMP (transit time magnetic pumping) fast wave current drive efficiency factor $\gamma \cong 0.11$ (in units of $10^{20} A/W/m^2$) can be obtained for $T_e = 10$ keV. However, if a 0.5% population of fast electrons (200 keV) is present in the central region of the plasma, values of γ in the range of 0.15 can be obtained as the lower part (n = 3-5) of the excited spectrum that resonates with the fast electrons has a higher current drive efficiency.

ACKNOWLEDGEMENT.

We wish to thank our colleagues in the JET team, especially the A2-antenna design team and the drawing office who have provided us the CAD generated drawings of the antenna sysytems. Discussions with C. Gormezano are appreciated. The help of J.J. Ellis in computational work is gratefully acknowledged. We thank V. Chen for providing us with his routine to calculate the current drive efficiency . We also thank D. Ehst for letting us use his analytic fit for the efficiency calculations.

REFERENCES.

[1] TUBBING, B.J.D. et al, APS Plasma Phys meeting, Tampa Florida, 1991.
[2] MOREAU, D. et al, Proc 14th Eur. Conf. on Contr. Fusion and Plasma Phys, Madrid, Spain, (1987) Europhys Conf. Abstracts, vol. III, 1007.
[3] START, D.F.H. et al, Nuclear Fusion, 30, 1990, 2170.
[4] PETTY, C.C. et al, Proc 9th Topical Conf on RF, Charleston, USA, 1991.
[5] START, D.F.H. et al, these proceedings.
[6] MAYBERRY, M.J. et al, Proc 9th Topical Conf on RF, Charleston, USA, 1991.
[7] BOSIA, G., these proceedings.
[8] HERSHKOWITZ, H. et al, Proc 9th Topical Conf on RF, Charleston, 1991.
[9] GOULDING, R.H. et al, Proc 9th Topical Conf on RF, Charleston, USA, 1991.
[10] BOSIA, G. et al, Fusion Technology, Vol 1, 1989, 459.
[11] BHATNAGAR, V.P. et al, Proc 9th Topical Conf on RF, Charleston, 1991.
[12] JACQUINOT, J. et al, Plasma Phys Contr Fusion, 1991 to be published.
[13] GORMEZANO, C. et al, these proceedings.
[14] VILLARD, L. et al, Ecole Polytechnique Federale de Lausanne, Suisse, Report CRPP INT 132/87 (1987).
[15] EDERY, D. et al, Association EURATOM CEA sur la Fusion, Cadarache, France, Report JET Art 14 contract JT5 9003, (1987).
[16] SMYTHE D. et al, Nuclear Fusion, 27, (1987), 1319.
[17] BHATNAGAR, V.P. et al, Nuclear Fusion, 22, (1982) 280.
[18] MESSIAEN, A. et al, Proc 3rd Grenoble-Varenna Int Symp, 1982, vol 1, 243.
[19] BRAMBILLA, M., Max-Planck Institute fur Plasmaphysik, Garching, FR Germany, Report IPP 4/210 (1983).
[20] LOBEL, R. et al, 16th Symposium on Fusion Technology, London, (U.K.), 1990, paper R26.

[21] BHATNAGAR, V.P. et al, JET Joint Undertaking, Abingdon, (U.K.), (1986) Report JET-R(86)05.
[22] BHATNAGAR, V.P. et al, Nuclear Fusion, 24, (1984) 955.
[23] CHIU, S.C. et al, Nuclear Fusion, 29, (1989) 2175.
[24] CORDEY et al, Plasma Physics, 24, (1982) 73.
[25] EHST, D.A. and KARNEY, C.F.F., Argonne National Lab., Argonne, (U.S.A.), 1990, report ANL/FPP/TM-247.
[26] KARNEY, C.F.F. et al, in Applications of Radiofrequency Power to Plasma (Proc. 8th Topical Conf. Irvine, 1989), McWilliams, R.
[27] BHATNAGAR, V.P. et al, Intn School of Plasma Phys, Varenna, Italy, Theory of Fusion Plasma, ISPP-6, 1990, 243.
[28] O'BRIEN, M.R., to be published in Nuclear Fusion, (1991).

Table 1 Plasma and antenna parameters used in the calculation.

PLASMA PARAMETERS		**JET**
Plasma composition		(He^3)-D
Minority concentration	n_{min}/n_{maj}	0
Z-effective		1
Toroidal field on axis	$B_0(T)$	3.08
Plasma Current	$I_P(MA)$	2
Operation frequency	f(MHz)	35
Central Electron Temperature	$T_{e0}(keV)$	10
Central ion Temperature	$T_{i0}(keV)$	4
Temperature profile exponent	p	1
Central plasma density	$n_{e0}(10^{19}m^{-3})$	5
Edge plasma density	$n_{es}(10^{19}m^{-3})$	0.8
Density profile exponent	ρ	0.85
Torus major radius	$R_0(m)$	3
Plasma radius	$a_p(m)$	0.97
Elongation	κ	1.5
Triangularity	δ	0.1
Shafranov shift	$\Delta_0(m)$	0
ANTENNA PARAMETERS		**A2**
Antenna conductor to limiter distance	a(m)	0.12
Antenna conductor to backwall distance	d(m)	0.25
Antenna conductor to screen distance	$x_{sc}(m)$	0.012
Length of one antenna element	w_y (m)	0.8
Half-width of the antenna element	$w_z(m)$	0.105
current propagation constant in y	$\beta(m^{-1})$	2
number of boxes energized	N_{box}	4
Number of antenna per box	N_y, N_z	2,4
Mid-line distance between two conductors	$L_z(m)$	0.4

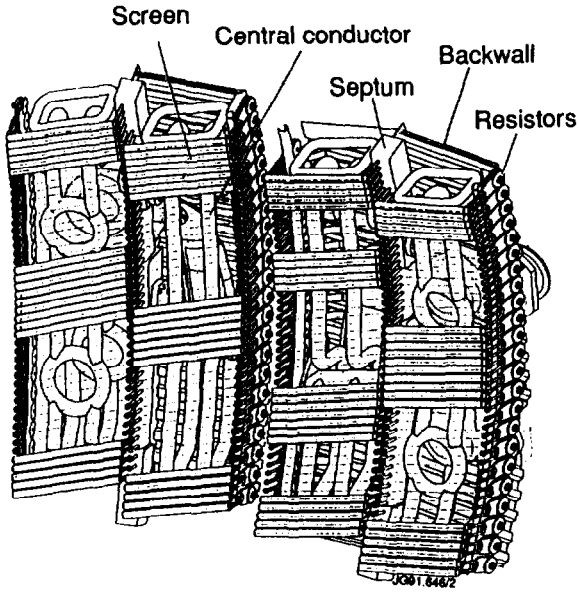

FIG. 1. A perspective view of a JET A2-antenna structure containing four current straps. Four such antennas will be mounted in the torus. Current strap frame is shown without the covering plates. (Courtsey of JET drawing office).

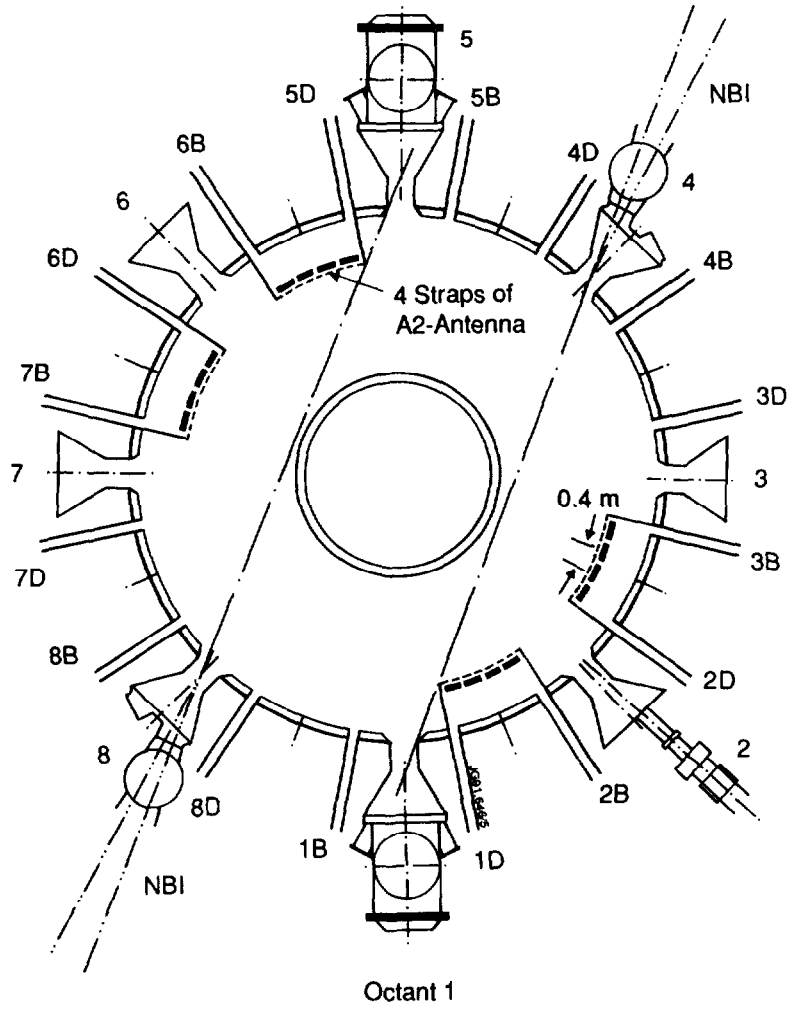

FIG. 2. A schematic drawing showing the A2-antenna locations in a plan view of the JET tokamak. Antenna locations are governed by the fixed beam line locations.

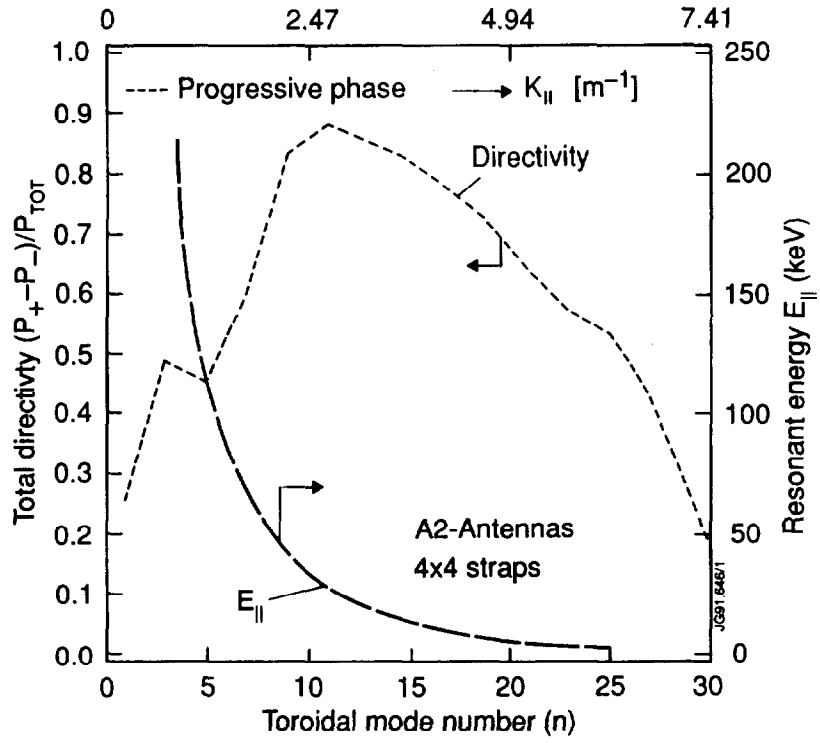

FIG. 3. A plot of the total directivity (for definition see text) as a function of the progressive phasing toroidal mode number n for the JET 4x4 A2-antenna locations given in Fig. 2. A corresponding $k_{//}$ scale is indicated on the top. Also the resonant parallel energy of electrons with a given $k_{//}$ is also shown for f = 35 MHz.

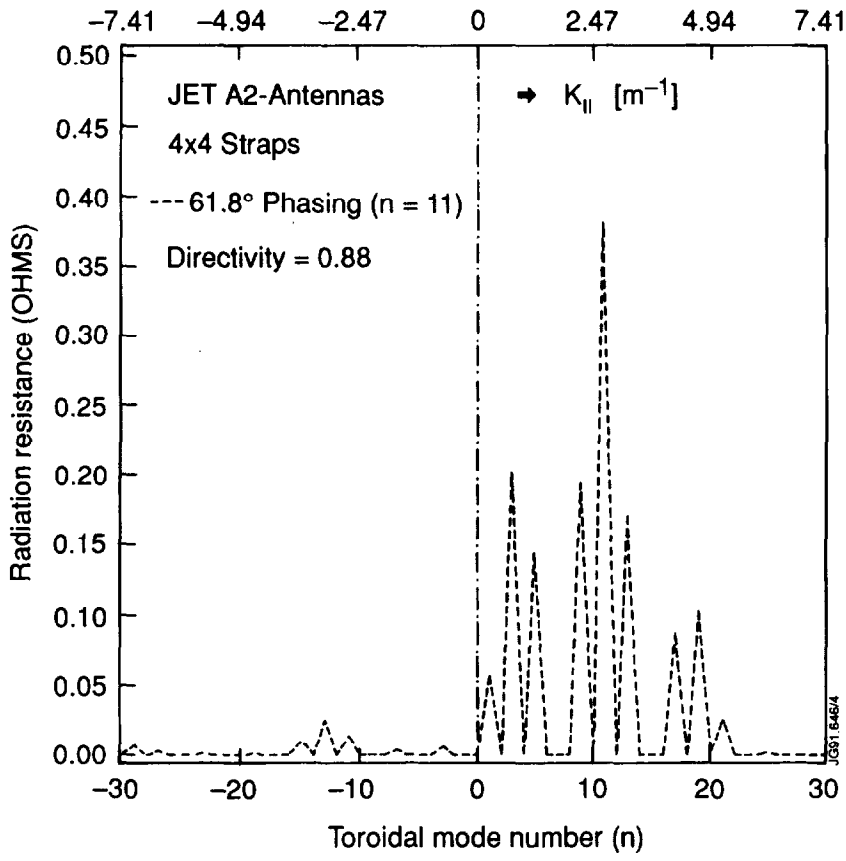

FIG. 4. Radiated power spectrum is plotted as a function of toroidal mode number n for a progressive phasing of 61.8° between two straps of a JET A2-antenna.

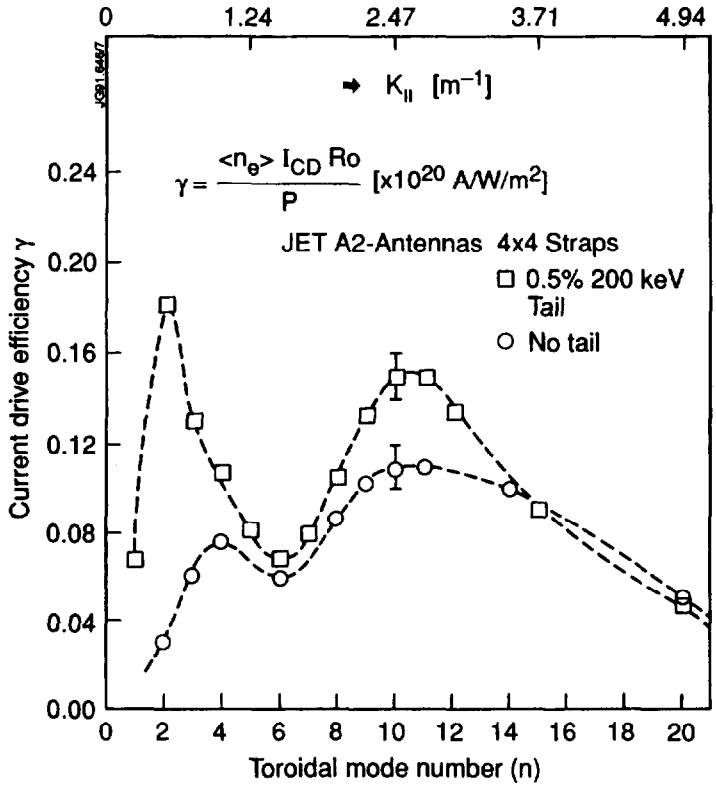

FIG. 5. A plot of the current drive efficiency factor γ as function of the toridal mode number n predominantly excited by the corresponding progressive phasing between straps of JET A2 antennas. Two cases are shown (1) with a 200 keV fast electron population present and (2) without the fast electrons.

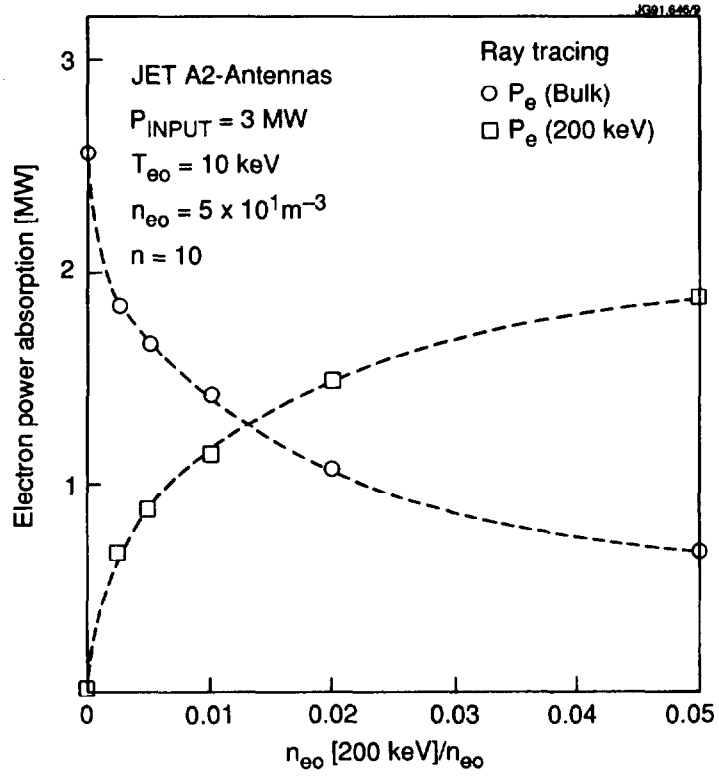

FIG. 6. A plot of the power absorbed by the bulk electrons and the 200 keV fast electron population as a function of the concentration of fast electrons for a phasing of n = 10 of JET A2-antennas.

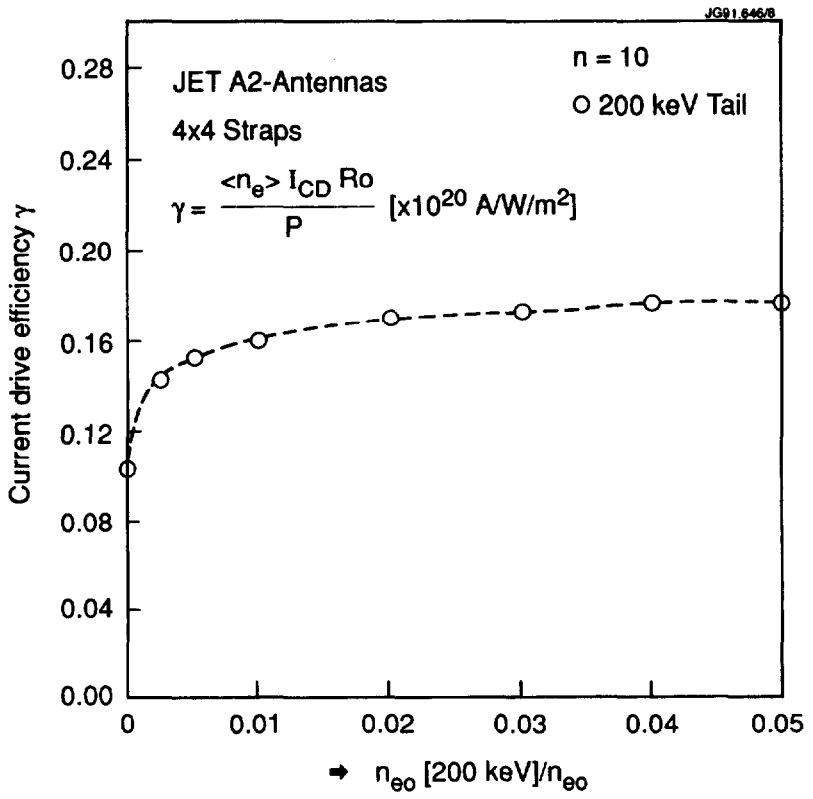

FIG. 7. A plot of γ as a function of the concentration of fast electrons for a phasing of n = 10 of JET A2-antennas.

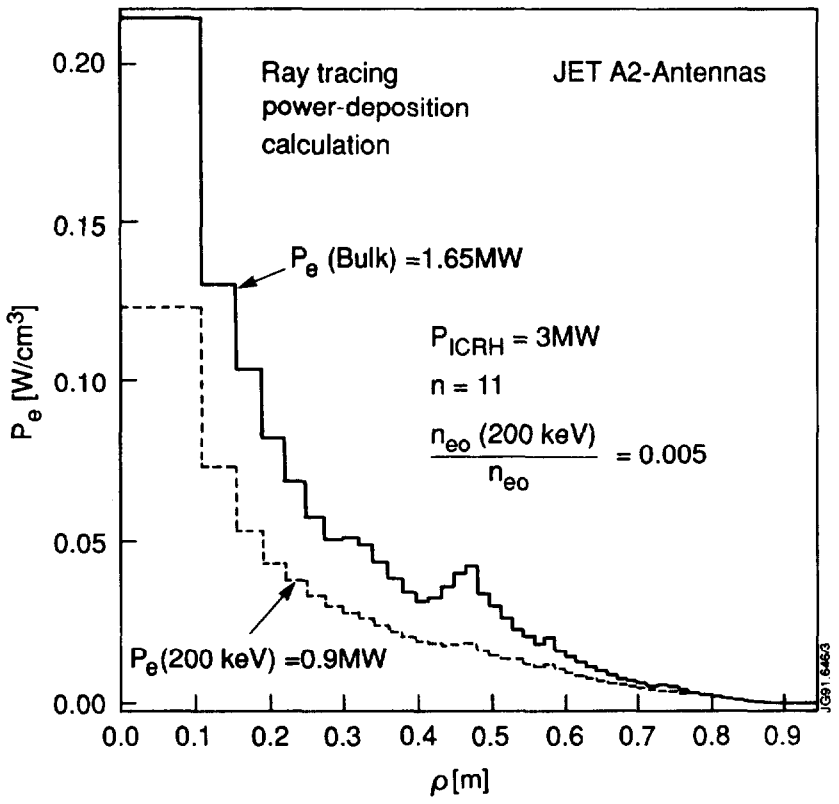

FIG. 8. A ray tracing generated deposition profile of the power absorbed by the bulk electrons and the 200 keV fast electron population for a phasing of n = 11 of JET A2-antennas.

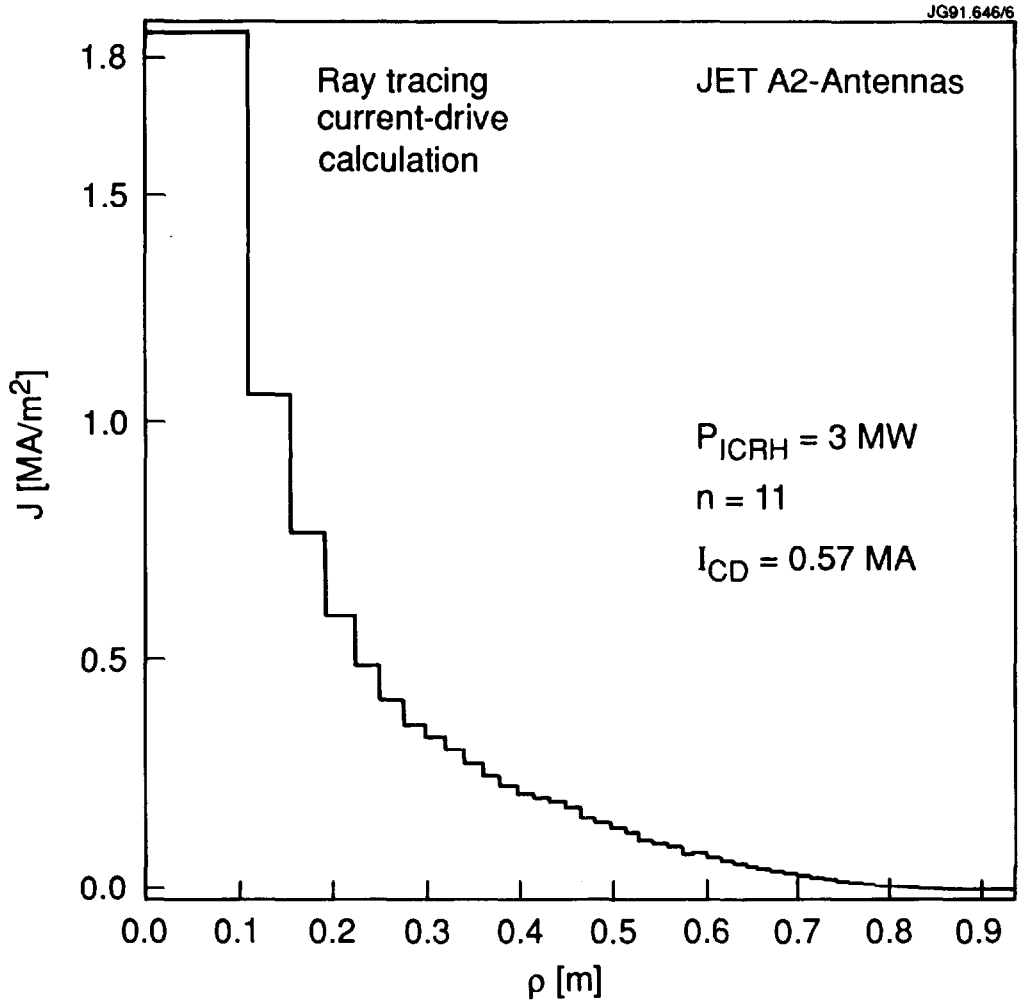

FIG. 9. A ray tracing generated ICRH driven current density profile in a case with the presence of 0.5% of fast electron population for a phasing of n = 11 of JET A2-antennas.

APPENDIX 1.

THE JET TEAM

JET Joint Undertaking, Abingdon, Oxon, OX14 3EA, U.K.

J.M.Adams[1], F.Alladio[4], H.Altmann, R.J.Anderson, G.Appruzzese, W.Bailey, B.Balet, D.V.Bartlett, L.R.Baylor[24], K.Behringer, A.C.Bell, P.Bertoldi, E.Bertolini, V.Bhatnagar, R.J.Bickerton, A.Boileau[3], T.Bonicelli, S.J.Booth, G.Bosia, M.Botman, D.Boyd[31], H.Brelen, H.Brinkschulte, M.Brusati, T.Budd, M.Bures, T.Businaro[4], H.Buttgereit, D.Cacaut, C.Caldwell-Nichols, D.J.Campbell, P.Card, J.Carwardine, G.Celentano, P.Chabert[27], C.D.Challis, A.Cheetham, J.Christiansen, C.Christodoulopoulos, P.Chuilon, R.Claesen, S.Clement[30], J.P.Coad, P.Colestock[6], S.Conroy[13], M.Cooke, S.Cooper, J.G.Cordey, W.Core, S.Corti, A.E.Costley, G.Cottrell, M.Cox[7], P.Cripwell[13], F.Crisanti[4], D.Cross, H.de Blank[16], J.de Haas[16], L.de Kock, E.Deksnis, G.B.Denne, G.Deschamps, G.Devillars, K.J.Dietz, J.Dobbing, S.E.Dorling, P.G.Doyle, D.F.Düchs, H.Duquenoy, A.Edwards, J.Ehrenberg[14], T.Elevant[12], W.Engelhardt, S.K.Erents[7], L.G.Eriksonn[5], M.Evrard[2], H.Falter, D.Flory, M.Forrest[7], C.Froger, K.Fullard, M.Gadeberg[11], A.Galetsas, R.Galvao[8], A.Gibson, R.D.Gill, A.Gondhalekar, C.Gordon, G.Gorini, C.Gormezano, N.A.Gottardi, C.Gowers, B.J.Green, F.S.Griph, M.Gryzinski[26], R.Haange, G.Hammett[6], W.Han[9], C.J.Hancock, P.J.Harbour, N.C.Hawkes[7], P.Haynes[7], T.Hellsten, J.L.Hemmerich, R.Hemsworth, R.F.Herzog, K.Hirsch[14], J.Hoekzema, W.A.Houlberg[24], J.How, M.Huart, A.Hubbard, T.P.Hughes[32], M.Hugon, M.Huguet, J.Jacquinot, O.N.Jarvis, T.C.Jernigan[24], E.Joffrin, E.M.Jones, L.P.D.F.Jones, T.T.C.Jones, J.Källne, A.Kaye, B.E.Keen, M.Keilhacker, G.J.Kelly, A.Khare[15], S.Knowlton, A.Konstantellos, M.Kovanen[21], P.Kupschus, P.Lallia, J.R.Last, L.Lauro-Taroni, M.Laux[33], K.Lawson[7], E.Lazzaro, M.Lennholm, X.Litaudon, P.Lomas, M.Lorentz-Gottardi[2], C.Lowry, G.Magyar, D.Maisonnier, M.Malacarne, V.Marchese, P.Massmann, L.McCarthy[28], G.McCracken[7], P.Mendonca, P.Meriguet, P.Micozzi[4], S.F.Mills, P.Millward, S.L.Milora[24], A.Moissonnier, P.L.Mondino, D.Moreau[17], P.Morgan, H.Morsi[14], G.Murphy, M.F.Nave, M.Newman, L.Nickesson, P.Nielsen, P.Noll, W.Obert, D.O'Brien, J.O'Rourke, M.G.Pacco-Düchs, M.Pain, S.Papastergiou, D.Pasini[20], M.Paume[27], N.Peacock[7], D.Pearson[13], F.Pegoraro, M.Pick, S.Pitcher[7], J.Plancoulaine, J-P.Poffé, F.Porcelli, R.Prentice, T.Raimondi, J.Ramette[17], J.M.Rax[27], C.Raymond, P-H.Rebut, J.Removille, F.Rimini, D.Robinson[7], A.Rolfe, R.T.Ross, L.Rossi, G.Rupprecht[14], R.Rushton, P.Rutter, H.C.Sack, G.Sadler, N.Salmon[13], H.Salzmann[14], A.Santagiustina, D.Schissel[25], P.H.Schild, M.Schmid, G.Schmidt[6], R.L.Shaw, A.Sibley, R.Simonini, J.Sips[16], P.Smeulders, J.Snipes, S.Sommers, L.Sonnerup, K.Sonnenberg, M.Stamp, P.Stangeby[19], D.Start, C.A.Steed, D.Stork, P.E.Stott, T.E.Stringer, D.Stubberfield, T.Sugie[18], D.Summers, H.Summers[20], J.Taboda-Duarte[22], J.Tagle[30], H.Tamnen, A.Tanga, A.Taroni, C.Tebaldi[23], A.Tesini, P.R.Thomas, E.Thompson, K.Thomsen[11], P.Trevalion, M.Tschudin, B.Tubbing, K.Uchino[29], E.Usselmann, H.van der Beken, M.von Hellermann, T.Wade, C.Walker, B.A.Wallander, M.Walravens, K.Walter, D.Ward, M.L.Watkins, J.Wesson, D.H.Wheeler, J.Wilks, U.Willen[12], D.Wilson, T.Winkel, C.Woodward, M.Wykes, I.D.Young, L.Zannelli, M.Zarnstorff[6], D.Zasche[14], J.W.Zwart.

PERMANENT ADDRESS

1. UKAEA, Harwell, Oxon. UK.
2. EUR-EB Association, LPP-ERM/KMS, B-1040 Brussels, Belgium.
3. Institute National des Récherches Scientifique, Quebec, Canada.
4. ENEA-CENTRO Di Frascati, I-00044 Frascati, Roma, Italy.
5. Chalmers University of Technology, Göteborg, Sweden.
6. Princeton Plasma Physics Laboratory, New Jersey, USA.
7. UKAEA Culham Laboratory, Abingdon, Oxon. UK.
8. Plasma Physics Laboratory, Space Research Institute, Sao José dos Campos, Brazil.
9. Institute of Mathematics, University of Oxford, UK.
10. CRPP/EPFL, 21 Avenue des Bains, CH-1007 Lausanne, Switzerland.
11. Risø National Laboratory, DK-4000 Roskilde, Denmark.
12. Swedish Energy Research Commission, S-10072 Stockholm, Sweden.
13. Imperial College of Science and Technology, University of London, UK.
14. Max Planck Institut für Plasmaphysik, D-8046 Garching bei München, FRG.
15. Institute for Plasma Research, Gandhinagar Bhat Gujat, India.
16. FOM Instituut voor Plasmafysica, 3430 Be Nieuwegein, The Netherlands.
17. Commissiariat à L'Energie Atomique, F-92260 Fontenay-aux-Roses, France.
18. JAERI, Tokai Research Establishment, Tokai-Mura, Naka-Gun, Japan.
19. Institute for Aerospace Studies, University of Toronto, Downsview, Ontario, Canada.
20. University of Strathclyde, Glasgow, G4 ONG, U.K.
21. Nuclear Engineering Laboratory, Lapeenranta University, Finland.
22. JNICT, Lisboa, Portugal.
23. Department of Mathematics, Univeristy of Bologna, Italy.
24. Oak Ridge National Laboratory, Oak Ridge, Tenn., USA.
25. G.A. Technologies, San Diego, California, USA.
26. Institute for Nuclear Studies, Swierk, Poland.
27. Commissiariat à l'Energie Atomique, Cadarache, France.
28. School of Physical Sciences, Flinders University of South Australia, South Australia SO42.
29. Kyushi University, Kasagu Fukuoka, Japan.
30. Centro de Investigaciones Energeticas Medioambientales y Techalogicas, Spain.
31. University of Maryland, College Park, Maryland, USA.
32. University of Essex, Colchester, UK.
33. Akademie de Wissenschaften, Berlin, DDR.

CR 88.49.1A